High-precision astrometry towards ELTs

Davide Massari[a,b], Giuliana Fiorentino[a], Eline Tolstoy[b], Alan McConnachie[c], Remko Stuik[d], Laura Schreiber[a], David Andersen[c], Yann Clénet[e], Richard Davies[f], Damien Gratadour[e], Konrad Kuijken[d], Ramon Navarro[g], Jörg-Uwe Pott[h], Gabriele Rodeghiero[h], Paolo Turri[i], and Gijs Verdoes Kleijn[b]

[a]INAF-Osservatorio Astronomico di Bologna, via Ranzani 1, 40127, Bologna, Italy
[b]University of Groningen, Kapteyn Astronomical Institute, NL-9747 AD Groningen, The Netherlands
[c]Herzberg Astronomy and Astrophysics, National Research Council Canada, 5071 West Saanich Road, Victoria, BC V9E 2E7, Canada
[d]Leiden Observatory, Leiden University, Postbus 9513, 2300 RA Leiden, The Netherlands
[e]LESIA, Observatoire de Paris, CNRS, UPMC, Université Paris-Diderot, 5 place Jules Janssen, 92195 Meudon, France
[f]Max-Planck-Institut für extraterrestrische Physik, Postfach 1312, D-85741, Garching, Germany
[g]NOVA Optical IR Instrumentation Group, P.O. Box 2, 7990 AA Dwingeloo, The Netherlands
[h]Max-Planck-Institut für Astronomie, Königstuhl 17, D-69117 Heidelberg, Germany
[i]Department of Physics and Astronomy, University of Victoria, 3800 Finnerty Road, Victoria, BC V8P 5C2, Canada

ABSTRACT

With the aim of paving the road for future accurate astrometry with MICADO at the European-ELT, we performed an astrometric study using two different but complementary approaches to investigate two critical components that contribute to the total astrometric accuracy. First, we tested the predicted improvement in the astrometric measurements with the use of an atmospheric dispersion corrector (ADC) by simulating realistic images of a crowded Galactic globular cluster. We found that the positional measurement accuracy should be improved by up to ~ 2 mas with the ADC, making this component fundamental for high-precision astrometry. Second, we analysed observations of a globular cluster taken with the only currently available Multi-Conjugate Adaptive Optics assisted camera, GeMS/GSAOI at Gemini South. Making use of previously measured proper motions of stars in the field of view, we were able to model the distortions affecting the stellar positions. We found that they can be as large as ~ 200 mas, and that our best model corrects them to an accuracy of ~ 1 mas. We conclude that future astrometric studies with MICADO requires both an ADC and an accurate modelling of distortions to the field of view, either through an a-priori calibration or an a-posteriori correction.

Keywords: Astrometry, Extremely Large Telescopes, Adaptive Optics, Globular Clusters

1. INTRODUCTION

Accurate astrometry is one of the major drivers for diffraction limited Extremely Large Telescopes (ELTs). To reach diffraction limited observations, the Multi-AO Imaging Camera for Deep Observations (MICADO), one of the first light instruments for the European-ELT, will be assisted by an Adaptive Optics module (MAORY,[1]) providing both a Single Conjugate (developed jointly with the MICADO consortium) and a Multi Conjugate modes. The goal of MICADO is a relative astrometric accuracy for bright and isolated stars of 50 μas over a

Further author information: (Send correspondence to D.M.)
D.M.: E-mail: davide.massari@oabo.inaf.it, Telephone: +39 051 2095318
G.F.: E-mail: giuliana.fiorentino@oabo.inaf.it, Telephone: +39 051 2095318

central, circular field of 20 arcsec diamater. To determine if such an ambitious goal is feasible, a dual approach is taken. To simulate stellar fields as they would be seen by the SCAO with the predicted instrumental Point Spread Function (PSF) and analyse the resulting realistic images will test the predicted performance, and help to optimise the instrumental design. In addition, present-day astrometric studies with existing MCAO facilities are crucial to test the main sources of inaccuracy not related to the specific instrumental design or telescope.

In this paper we present both these approaches, as complementary studies. In particular, we start by investigating in Section 2 how to best reach the astrometric requirement for MICADO by quantifying the errors associated to one of the most important components in the light path: the atmospheric distortion corrector (ADC). This investigation is carried out making simulations with the SCAO module PSF of the central region of a crowded globular cluster, for a field of view of 2×2 arcsec. This size is small enough for PSF variations not to be important, but big enough to contain a sufficient number of stars.

Then, in Section 3, we also present the results of an astrometric study performed with Gemini Multi-Conjugate Adaptive Optics System (GeMS) observations of the Galactic globular cluster NGC6681. This cluster is the most centrally concentrated in the Galaxy, and thus represents a major observational challenge in terms of stellar crowding. We have previously determined proper motions by comparing two Hubble Space Telescope epochs ([2]). This makes this cluster an ideal candidate to test the effects that will be introduced by MCAO corrections on proper motion measurements and related uncertainties. In particular, we looked for systematic distortions introduced in the GeMS images by observing through both J and Ks filters and we quantify their impact on the astrometry. Though previous studies have already tested the astrometric performance of MCAO cameras (e.g.[3–6]), our investigation is the first to address the detailed structure and sizes of distortions in a MCAO instrument and will therefore be the starting point for understanding MCAO astrometry capabilities and any future improvements in the calibration and data reduction strategy for ELT observations.

2. MICADO ADC SIMULATIONS

One of the most severe observational issues concerning accurate astrometry is *atmospheric dispersion*. Since the refractive index of the atmosphere, n, depends on the wavelength, the observed angular distance between two sources is altered depending on the difference of their colours. Moreover, atmospheric dispersion elongates the shape of the PSF along the zenith, thus reducing the Strehl ratio and affecting the precision of any astrometric measurement. This is especially true in crowded fields, where the position of faint sources is affected by the broader wings of the PSF of bright neighbours. Since the combined effect can have an impact as large as few mas on the astrometry ([7]), an adequate correction is mandatory. Previous dedicated studies determined as best solution for MICADO observations to introduce a counter-rotation based ADC located at the pupil of the instrument. A detailed description of such a component is provided in an internal communication document by Remko Stuik.

In order to quantify the impact of using an ADC on the astrometric performances of MICADO, we simulated realistic images of a Galactic globular cluster field using the predicted instrumental PSF of the SCAO module. The PSF were generated from a preliminary set of AO simulations on the COMPASS platform by Yann Clenet ([8]). The telescope spiders and segmentation were added to the individual frames and the PSF was shifted based on wavelength and zenith angle. An optical ZEMAX model was used to compute the correction as a function of wavelength for an ideal ADC with counter-rotating double prisms, assuming a fixed zenith angle of 60 degrees. We stress that this is not a full end-to-end model, and that the interactions between all of the various sources of error, as well as optical and alignment errors, are not fully included. The PSFs were computed on axis, in the standard Ks-band filter, with an atmospheric coherence length $r_0 = 0.129$ m at a wavelength of 0.5 μm and a resulting Strehl ratio of 0.76. The AO simulations ran for 1 hour, with a frame rate of 1 kHz, but only one of every 1000 PSF images was saved. Therefore, each PSF of 1 ms represents 1 s of data. To perform our astrometric tests, we summed N independent PSF realisations to produce exposures of N seconds. Although the global PSF is a correct representation of the stated exposure time, the noise statistics are not. The PSF predicted for a 20 s MICADO exposure without (a-panel) and with the inclusion of the ADC in the light path (b-panel) are shown in Figure 1.

It is already clear that the ADC can correct the PSF, making it more symmetric and removing many of the speckles near the upper region of the PSF core. The PSF also appears sharper, with a Strehl ratio that increases

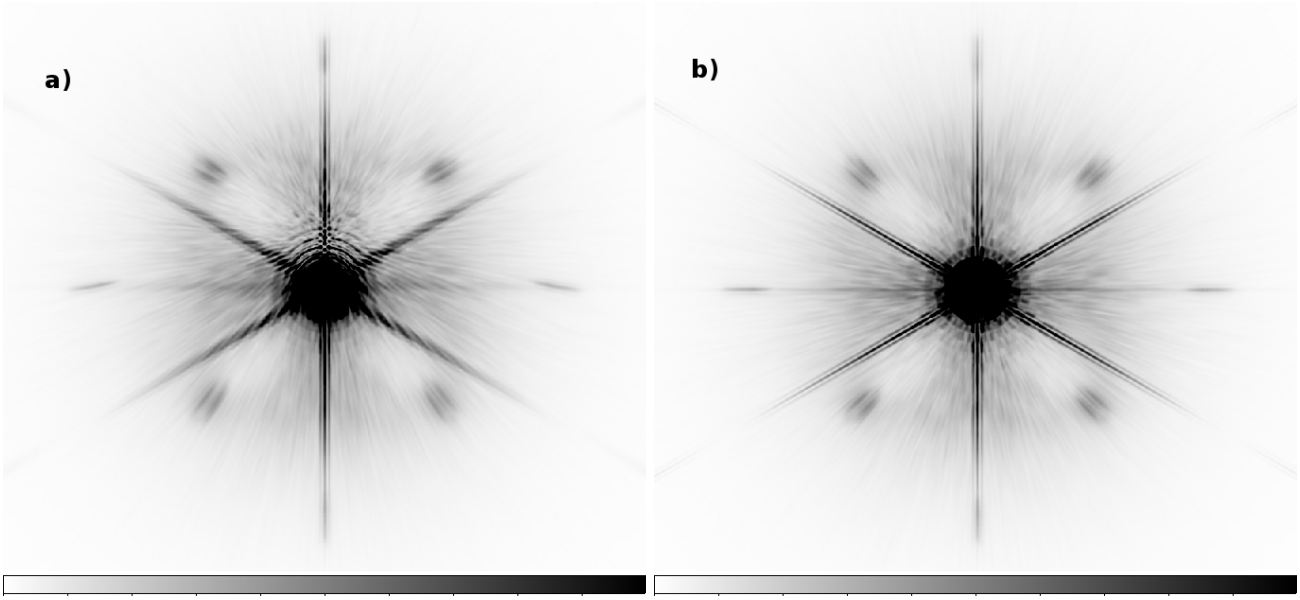

Figure 1. Comparison between the PSFs predicted for a 20 s MICADO exposure without (Figure 1a) and with (Figure 1b) the inclusion of an ADC in the light path. Each image has a size of 4096 × 4096 pixels and is orientated with the X and Y axis corresponding to Right Ascension and Declination, respectively.

from 0.35 to 0.76. In the following we will quantify the astrometric improvement due to the introduction of the ADC, demonstrating how fundamental this component is for astrometric studies of crowded stellar fields with MICADO.

2.1 Input catalogue and Simulations

To carry out our investigation, we simulate a realistic astrophysical problem. A natural choice is the crowded stellar field of a Galactic globular cluster (GC). In fact, GCs have routinely been the subject of detailed astrometric studies (e.g.[9,10]), and because of the availability of bright guide stars, they are ideally suited to be studied with diffraction-limited AO observations. In our investigation we want to simulate only a small region of the sky, where the PSF can reasonably be assumed to be constant across the entire field of view (FoV). Several previous studies have demonstrated that the PSF in AO images varies in a way that is very difficult to predict (see e.g.[11–14]). However, the introduction of a variable PSF is beyond the current scope of this work and will be addressed in future investigations. At the same time, we need to simulate a number of stars large enough to draw statistically significant conclusions. For these reasons, we choose to simulate the innermost 2 arcsec × 2 arcsec region of the crowded core of the GC M3 ([15]). Since M3 is known to have a flat density distribution in its core ([16]), it is correct to assume that stars are uniformly distributed in the central 2 arcsec × 2 arcsec region, and we can build the input catalogue simply by distributing the stellar positions randomly.

We determined the realistic number of stars to be simulated using the Hubble Space Telescope (HST) catalogue of M3 ([17]). After correcting it for incompleteness effect, we found the total number of stars in our FoV to be ~ 650. This is the population we will use to create a realistic simulation of a MICADO image of M3. We also reproduced a realistic distribution of stellar magnitudes by using the theoretical models taken from the Basti archive ([18]).

The software used to create the simulated images is described in detail in.[19] A few of the technical specifications used in that paper were updated for this investigation. In particular, we now use a primary mirror with an outer diameter of 37.0 m, an 11.1 m internal diameter, 6 spiders of 40 cm width every 60 degrees, for a total

effective area of 947.3 m^2. Given a pixel-scale of 3 mas/pixel* our 2×2 arcsec images have a size of 667×667 pixels. We created two sets of simulated images, with and without the inclusion of the ADC, with exposure times of 2 s, 4 s, 5 s, 10 s, 20 s and 120 s. These images were built following a random dither pattern to reproduce a typical scientific observation. An example of an image simulated in this way and using a 20 s exposure PSF with ADC is shown in Figure 2.

2.2 Astrometric analysis

The source detection and extraction in the simulated images has been carried out with the DAOPHOT ([20]) suite of software. The PSF model used to fit the light profile of each star was determined on the images, without exploiting any a-priori knowledge. This is to accurately mimic what happens routinely when dealing with real imaging data. Here, the best solution turned out to be a Moffat function. No degrees of spatial variation were necessary, since by construction the PSF does not vary across the images FoV. This model was then fit to all of the sources above a 3σ threshold of the sky background by ALLSTAR, to give a catalogue of stellar positions and instrumental magnitudes as output.

The first interesting result comes from a comparison of the number of input sources with the number of sources actually recovered in the analysis, that is a sort of completeness test (see also[19,21] for other detailed analysis on the achievable completeness with simulated MICADO data). The achieved completeness is shown in Figure 3. It does not take into account false detections, which are stars found that were not in the input list, and were discarded by cross-matching input and output catalogues.

As expected due to the superior PSF quality, the performance obtained in the ADC-case is strikingly better than that without the ADC. This shown in Figure 4. In the ADC-case (left panel of Figure 4) the software is able to pick up most of the true sources (plus some PSF artefacts that however can be easily identified and discarded because of their non-stellar shape). In contrast, in the no-ADC case (right panel of Figure 4) the elongated PSF causes the fainter stars to fall below the detection limit, while bright stars with bright companions can often no longer be recognised as independent sources. This is already an important indication of how important it will be to have an ADC assisting MICADO at the E-ELT, not only for astrometry but also for purely photometric purposes.

We tested the astrometric performance by comparing the input positions with those recovered by the software as output. In particular, we considered all of the stars in a given exposure, and computed the root mean square (rms) of the difference between input and output positions. Then, we divided our sample of stars in bins of magnitude and computed the corresponding mean rms value. Magnitude bins were defined in order to have a statistically significant number of stars (at least 70) in each of them. Finally, we determined the difference of the rms values between the non-ADC and the ADC case, and we show its behaviour with respect to exposure time and input magnitude in the two panels of Figure 5. The X- and Y- direction of the detector have been analysed separately.

The improved performance with the inclusion of the ADC is marked. This is especially evident in the Y-component (upper panel of Figure 5), since it is the direction where the atmospheric dispersion most affects the PSF shape in our simulations because of our chosen field orientation. The difference in the performances in the X-direction is less conspicuous, but clearly improving for fainter magnitudes and shorter exposure times. Of course for real observations without the ADC, such a distortion usually has a significant component in both the directions depending on the orientation, thus affecting strongly the achievable astrometric accuracy in both axes. When combining in quadrature the improvement in both components, our tests reveal that the minimum improvement (obtained with the brightest stars in the longest exposure) amounts to $\sim$ 370 μas, while the maximum value (for the faintest stars in the shortest exposure) amounts to $\sim$ 2000 μas, in fair agreement with the prediction of.[7] Therefore, under the hypothesis that the PSFs used are realistically reproducing the reliable effect of the ADC, our study strongly supports the need of a high-functioning ADC in MICADO to achieve accurate astrometry.

*Note that the current predicted diamater of the E-ELT is 38.5 m, while the MICADO pixel-scale is currently set to 1.5 mas/pixel for the high spatial resolution mode.

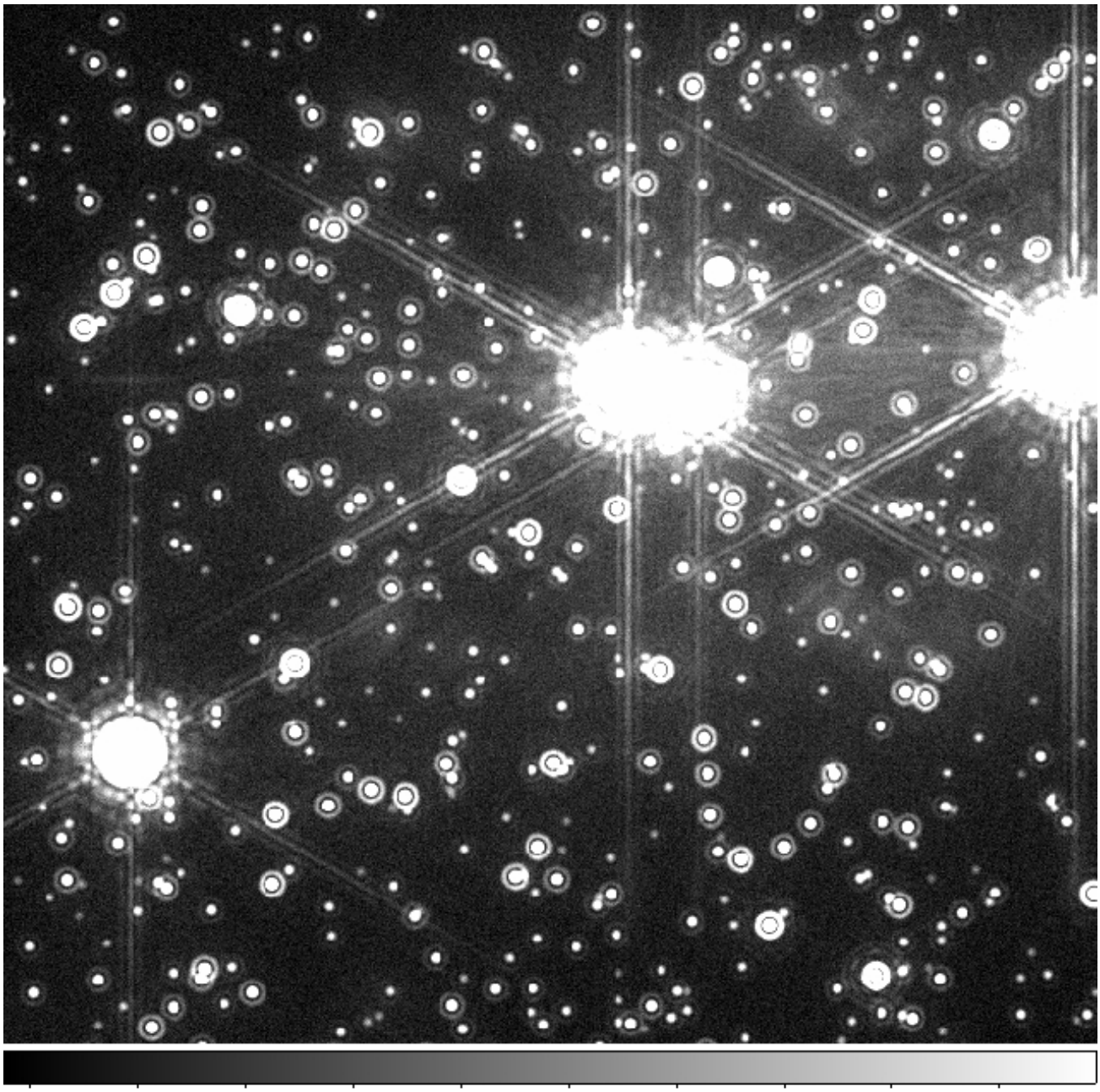

Figure 2. Example of one of the simulated stellar field analysed in this work. The image simulates a 20 s exposure of the inner 2×2 arcsec of the GC M3 taken in the Ks band with MICADO, with the inclusion of the ADC.

2.3 Discussion on the astrometric accuracy

As stated in the Introduction, MICADO has the ambitious goal of reaching a relative astrometric accuracy of 50 μas for bright and isolated stars. To reach such a goal, all of the components of the instrumental design have to be carefully tested in order to minimise the contribution of any systematic source of astrometric error to the overall budget. In this investigation, we focused on the impact that the ADC has on the SCAO performance of MICADO in simplified conditions, namely that the simulated FoV is small and on axis, and without considering

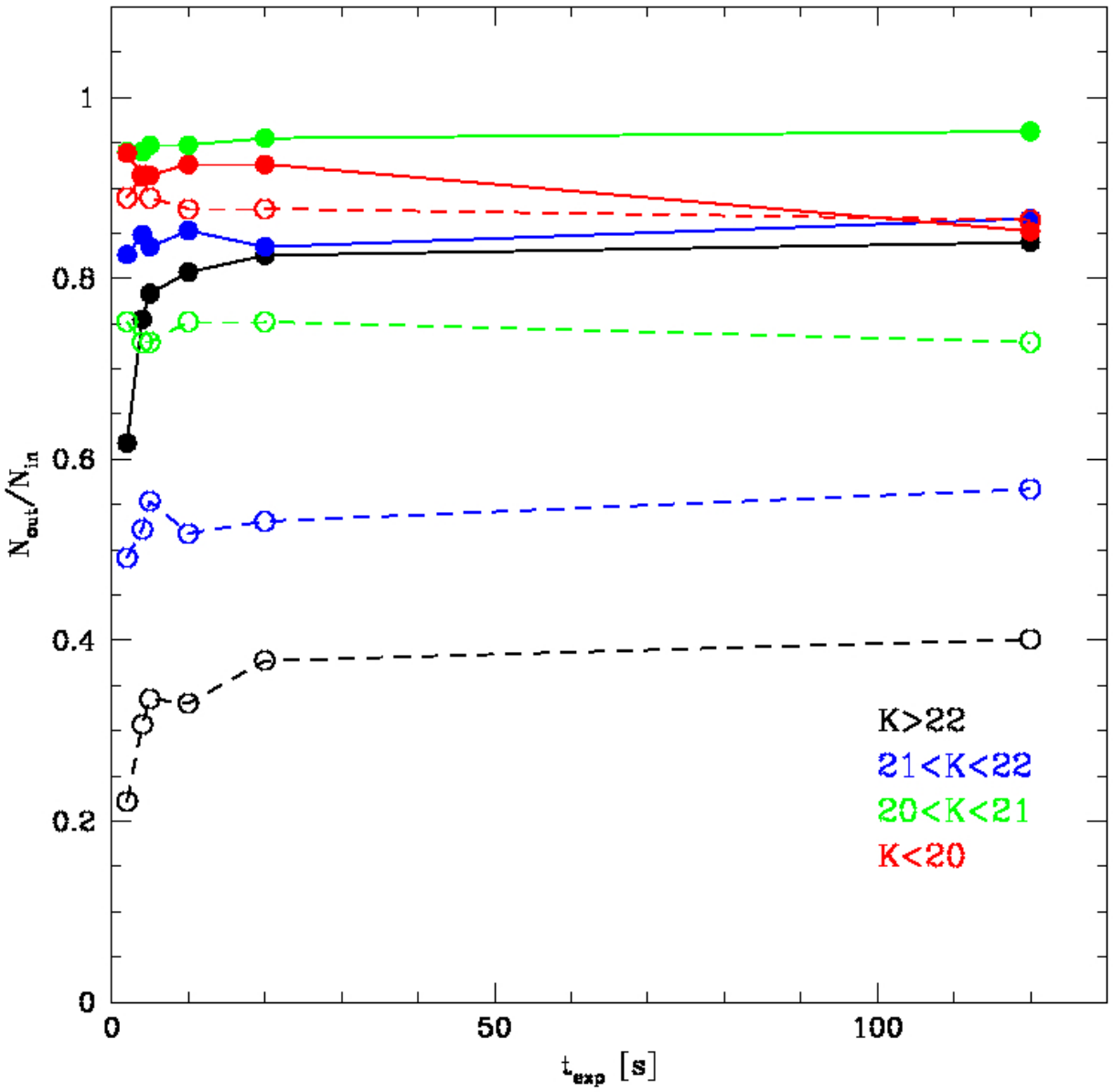

Figure 3. Completeness as a function of exposure time and stellar magnitude. Filled symbols connected by solid lines mark the results for the simulations including the ADC. Empty symbols connected by dashed lines those for the simulations without the ADC. Different bins of magnitude are shown with different colours, as explained in the labels.

the effects of the camera distortions, but for a realistic observational setup and science case. Our findings clearly demonstrate that the inclusion of the ADC is a fundamental requirement to reach high-precision astrometry, since in the simulated conditions it significantly improves the astrometric performance by at least ~ 370 μas.

One of the future goals we will pursue is to improve the PSF generation, including the realistic ADC manufacturing errors together with the instrumental ones. Another necessary future step is to accurately quantify the total contribution of the ADC to the overall astrometric error budget. To do so, we also need to quantify

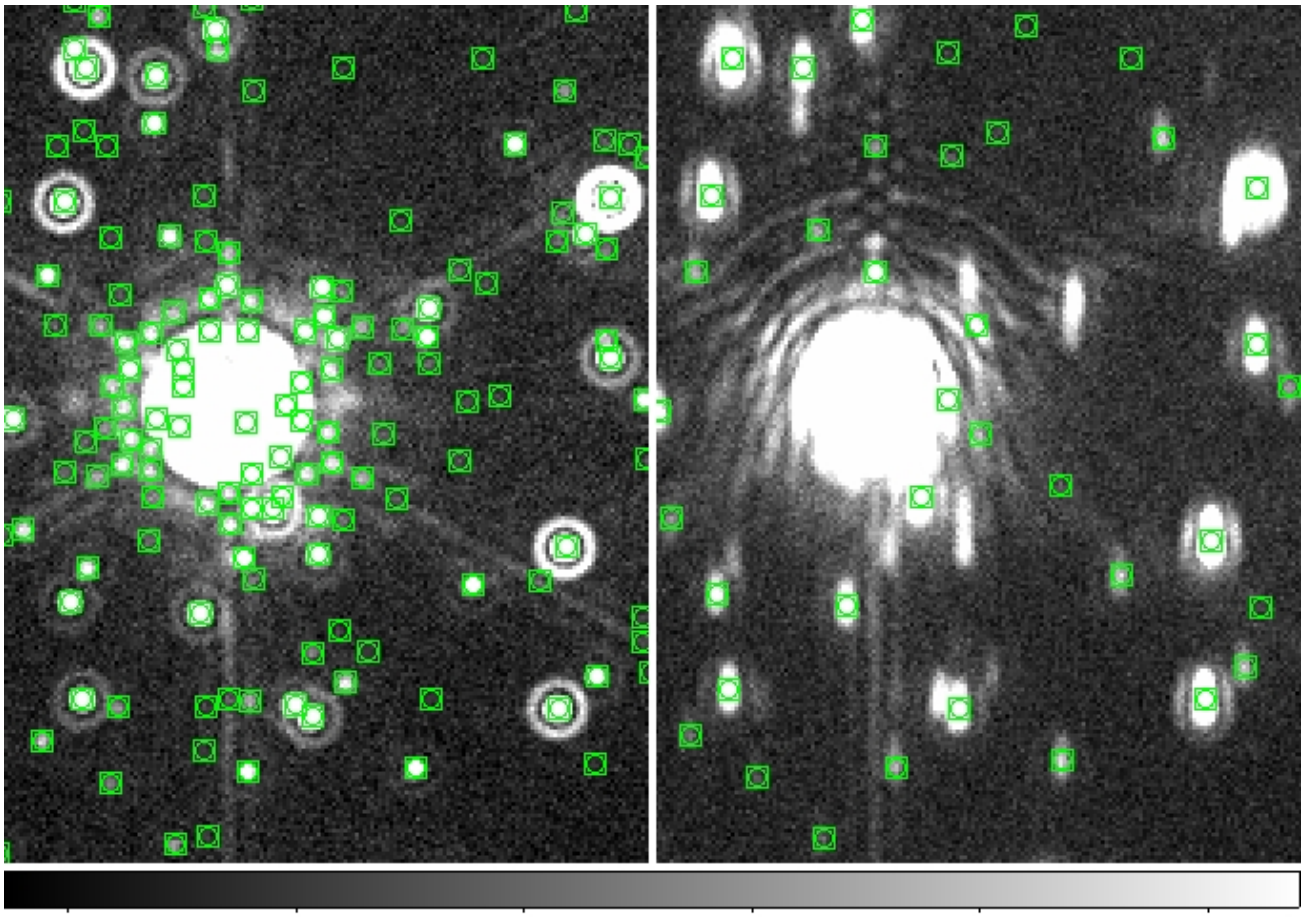

Figure 4. 190 × 230 pixels zoomed region of one of the simulated images. Left panel shows the simulation with the inclusion of the ADC, and vice versa. Green symbols show the sources recovered by the reduction software. For all these simulations, the direction of the PSF distortion coincides with the Y component of the detector.

the contribution to the error coming from the inability of current software in modelling the PSF. Starfinder ([22]) is the ideal software to do this, as it is able either to model the PSF directly on the single frames, or to use as input the same PSF used to simulate the images, thus bringing to zero the uncertainty due to the PSF modelling. However, we stress that the procedure we followed in this study is routinely and necessarily followed when analysing real images given that no sufficiently accurate a-priori knowledge of the PSF is usually available, the only exception being PSF reconstruction experiments (e.g.[23]). Once the intrinsic contribution to the astrometric error budget from the optical design, including the ADC, is estimated, we will also be able to quantify the potential effects of the reduction software. This will be extremely important in order to determine what are the likely future software requirements, and to test how PSF reconstruction techniques could reduce the overall astrometric uncertainty budget.

3. REAL DATA

The practical requirement to measure stellar proper motions (PMs) is to determine the displacement of stellar positions between two (or more) epochs. However, the physical motion of a star is not the only contribution to such a displacement. In fact, any effect artificially altering the observed position of a star with respect to the true one introduces a "distortion"that, without a proper treatment, is degenerate with the PM signal. For this reason it is fundamental to disentangle the effect of such distortions before any astrometric investigation.

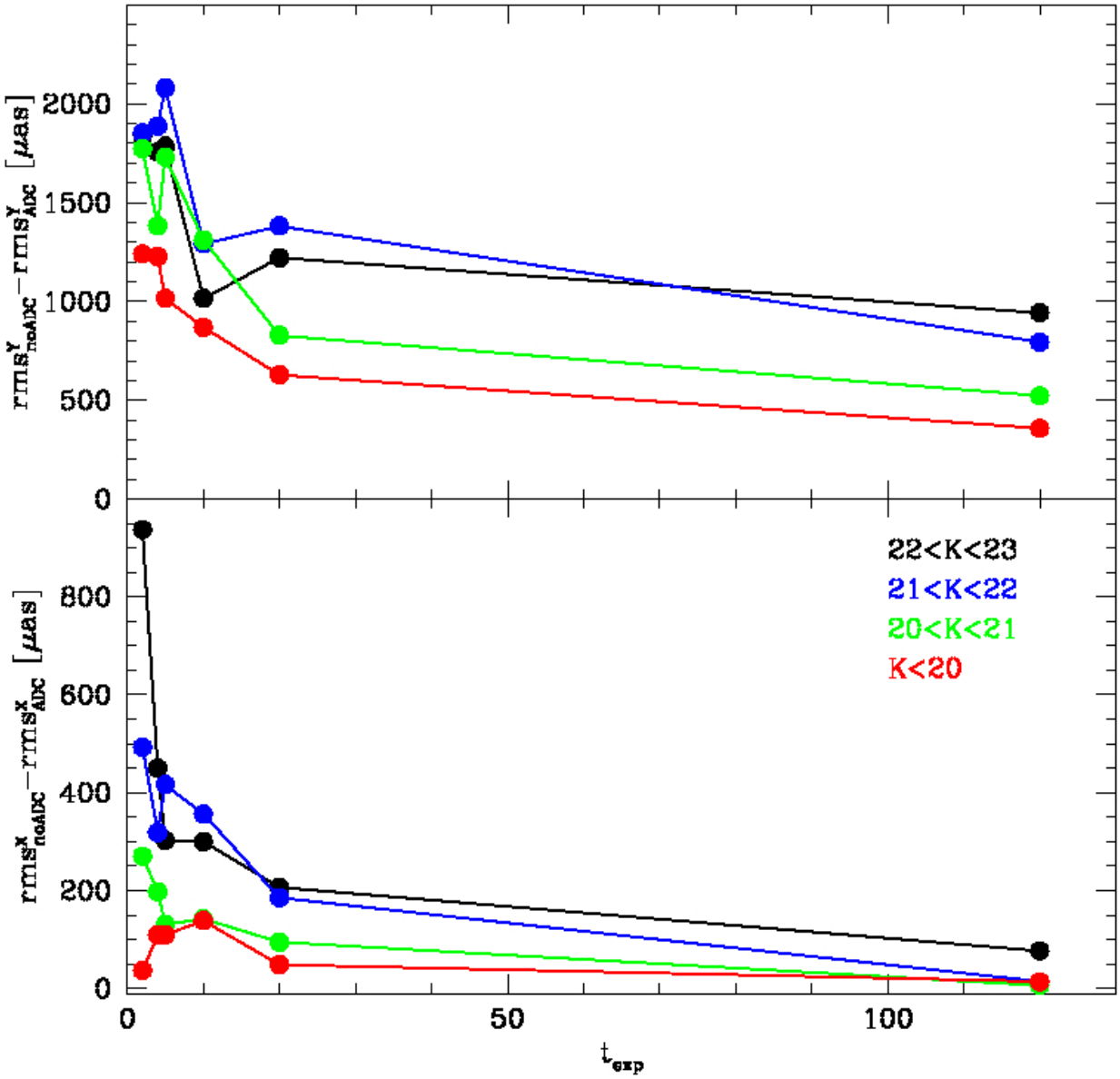

Figure 5. Difference between the astrometric performance between the no-ADC and the ADC case as a function of exposure time and stellar magnitude (see the labels). Symbols are colour-coded as in Figure 3. The larger difference found in the Y-direction of the detector is due to the direction of the PSF distortion in our simulations.

In this respect, MCAO systems are particularly complex to deal with. In fact, deformable mirrors conjugated to high altitude layers far away from the pupil can induce field distortions that significantly affect the overall astrometric accuracy (see e.g. the discussion in[3]). Since the magnitude and structure of distortions in MCAO data might change with differing seeing conditions, asterisms, airmass ([5,24]) and are as yet poorly investigated, our ability to determine how accurately they can be corrected remains uncertain. Calibrating the camera distortions and applying the general solution to any data-set is unlikely to prove sufficiently accurate for high-precision astrometric studies, because the distortions change from case to case. One of the possible solution to

this problem, would be to correct each exposure of a data-set with its own absolute solution, but this requires the availability of a distortion-free reference to break the PM-distortion degeneracy.

In the meantime a case where we can still make an accurate assessment of these effects is the Galactic GC NGC6681. This is because, both the distortion free positions in a past epoch and the PMs of the stars in the cluster FoV are known from Hubble Space Telescope (HST) measurements (,[2] hereafter Ma13). Recent observations have been taken with the MCAO camera GeMS ([25]) for this cluster (Programme IDs: GS-2012B-SV-406, GS-2013A-Q-16, GS-2013B-Q-55, PI: McConnachie). Therefore, in this case we have all of the necessary ingredients to determine the distortions caused by the MCAO on the GeMS camera.

3.1 The method

Because we have distortion-free stellar positions at the epoch of the first HST measurement (GO:10775, PI:Sarajedini) and their PMs from subsequent HST epochs (Ma13), it is possible to build a distortion-free reference frame at the epoch of GeMS observations. In this way, the differences between the observed GeMS positions and those from HST projected at the GeMS epoch are only due to distortion terms.

In order to be as accurate as possible, only NGC6681 stars with a PM uncertainty smaller than 0.03 mas yr^{-1} were used to build the reference frame. Their large number (7770) allow us to accurately sample the area in common between the HST and the GeMS data sets.

The distortion-free reference at the GeMS epoch were aligned in Right Ascension (RA) and Declination (Dec), and then all the GeMS exposures were registered to this reference frame to estimate their distortion maps. The GeMS data set is composed of 8×160 s exposures in both the J and the Ks filters, dithered by a few, non-integer pixel steps to cover the intra-chip gaps of the camera and to allow a better modelling of the PSF. All of the details concerning the reduction of the images will be described in a forthcoming paper (Massari et al. in prep.). Briefly, stellar raw positions (x_i^r, y_i^r) were obtained via PSF fitting using the DAOPHOT suite of software ([20]) and following the procedure described in.[14] Each of the four chips of the camera was treated separately. The PSF best-modelling was achieved by fitting the light profile of several hundred bright, isolated stars with a Moffat function and allowing the fitting residuals to be described with a look-up table that varies cubically across the FoV. By matching each exposure raw positions to the distortion-free reference using a 5th-order polynomial, the corrected, distortion-free GeMS positions (x_i^c, y_i^c) were obtained.

The 5th-order polynomial turned out to be the best choice when trying to balance the improvement of the rms of the transformations. This was determined by attempting to keep the order as low as possible, so as not to introduce spurious effects due to excessive degrees of freedom. In particular, when moving from the third order to the fourth and fifth, the rms of the transformations improved by $\sim 4\%$ per order, leading to a final rms of ~ 1 mas. Instead, for the following orders the improvement was only by $\sim 1\%$.

3.2 Quantifying GeMS distortions

The aim of this analysis was to quantify the distortions that affect GeMS astrometry. We stress that the contribution to these distortions does not come only from the instrumental geometric distortion, but also from all of the effects that artificially alter the position of a star such as anisoplanatism effects or an imperfect PSF modelling, and thus affect our ability to measure the true PM of that star. The average GeMS distortion maps for the J and Ks images are shown in Figure 6. Each single exposure distortion map was built as the difference between the positions corrected with the 5th- order polynomial (x_i^c, y_i^c), and the positions corrected using only linear transformations (thus taking into account rigid shifts, rotations and different scale). For the upper left corner of the camera, the polynomial solution is extrapolated, since no stars in common with the HST FoV of Ma13 were found. Therefore the solution in that small area might not be representative of the true distortions. For all of the stars in common to all of the eight exposures per filter, the difference vectors were averaged and then multiplied by 20 to enhance the details.

Several structures in the distortion maps are in common among all of the chips and both the filters. The amplitude of the distortions in the X-component (corresponding to RA) is significantly larger than that in the Y-component (Dec). In fact the former spans an interval ranging from -1.86 pixels to 4.83 pixels (mean value of 0.6 pixels), while the latter varies from -0.82 pixels to 0.52 pixels (mean value of -0.01 pixels). The corners

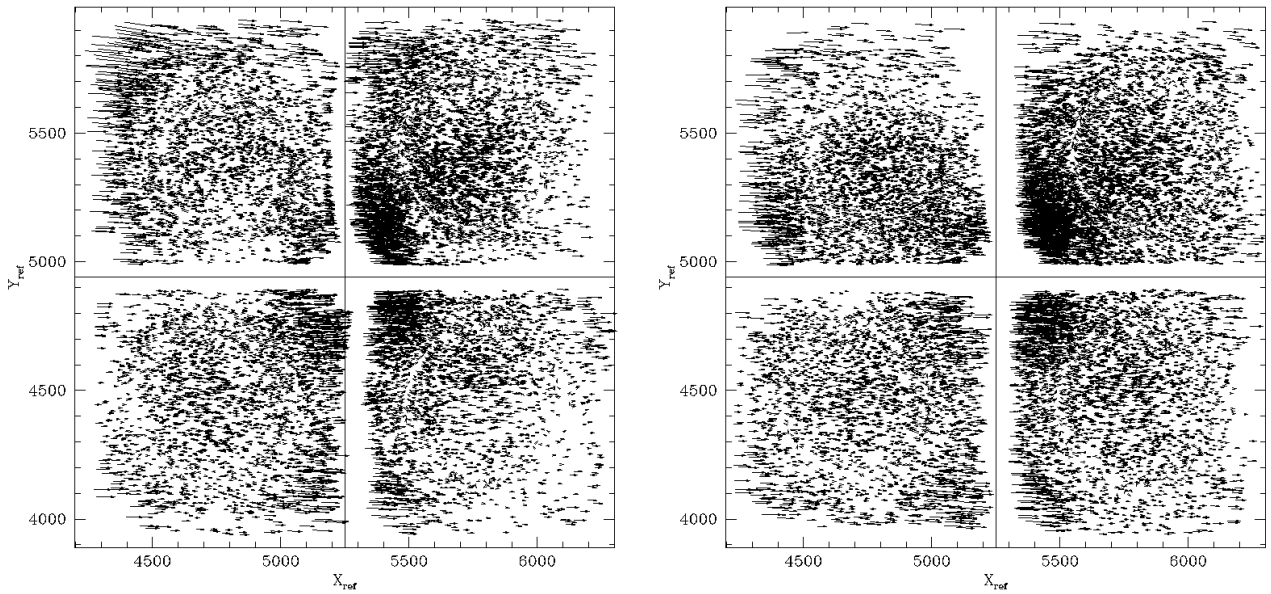

Figure 6. Average distortion maps for the J filter (left panel) and Ks filter (right panel). Vectors length is multiplied by a factor of 20 to highlight the distortion structures.

of each chip appear to be more distorted. Since the size of each pixel is that of the HST/ACS, the largest distortions are of the order of 0.2 arcsec. Similar values were found independently on another GeMS data set (S.Saracino, private communication). A quite striking common feature is a circular structure roughly located at the centre of each chip (which does not move from exposure to exposure) where the X-component distortion changes its sense. Another remarkable feature is the similarity of the distortions in the four separated chips. Not only the structure, but also their magnitude is very similar. For all the four chips, minimum, maximum and mean distortion values in X and Y agree within ~ 0.1 pixels

Finally, to separate the distortion component that changes from exposure to exposure, we build residual maps, that is the difference between each single distortion map and the average one of the corresponding filter. An example for a K-band exposure is shown in Figure 7. In the left-hand panel each vector is multiplied by a factor of 20, and the good work made by the average map in describing the overall behaviour of the single-exposure map is evident. In the right-hand panel, instead, the vectors are multiplied by a factor of 80, to enhance the residuals. The main structures observed in the average maps have disappeared, and only a different pattern survive. The magnitude of the residual distortions are again very similar among each chip, and ranges from -1.1 pixels to 1.3 pixels (mean value 0.05 pixels) in the X component, and from -0.11 pixels to 0.07 pixels (mean value 0.0 pixels) in the Y component. Note that by excluding the most external corners, the variation ranges are much smaller, being limited between -0.02 to 0.03 pixels in both components. Since from exposure to exposure the only significant difference is the seeing, we interpret these residual maps as the distortion variations introduced by the varying observing conditions. This will likely play a significant role in our ability to carry out accurate astrometry and photometry, and will need to be further studied.

3.3 Discussion on the distortion maps

Using previous PM studies with HST we were able to acquire a-priori knowledge to break the PM-distortions degeneracy for GeMS observations of the GC NGC6681, and are thus able to model the time varying distortions of each exposure taken with the MCAO-assisted camera. Our findings show that the average distortion across the entire FoV amounts to ~ 30 mas, but it can reach values as large as ~ 200 mas. With the use of a fifth order polynomial, we were able to model the distortion to an accuracy of ~ 1 mas. A contribution to this term is given by the propagation of the PM error of the stars used to build the distortion-free reference frame at the GeMS

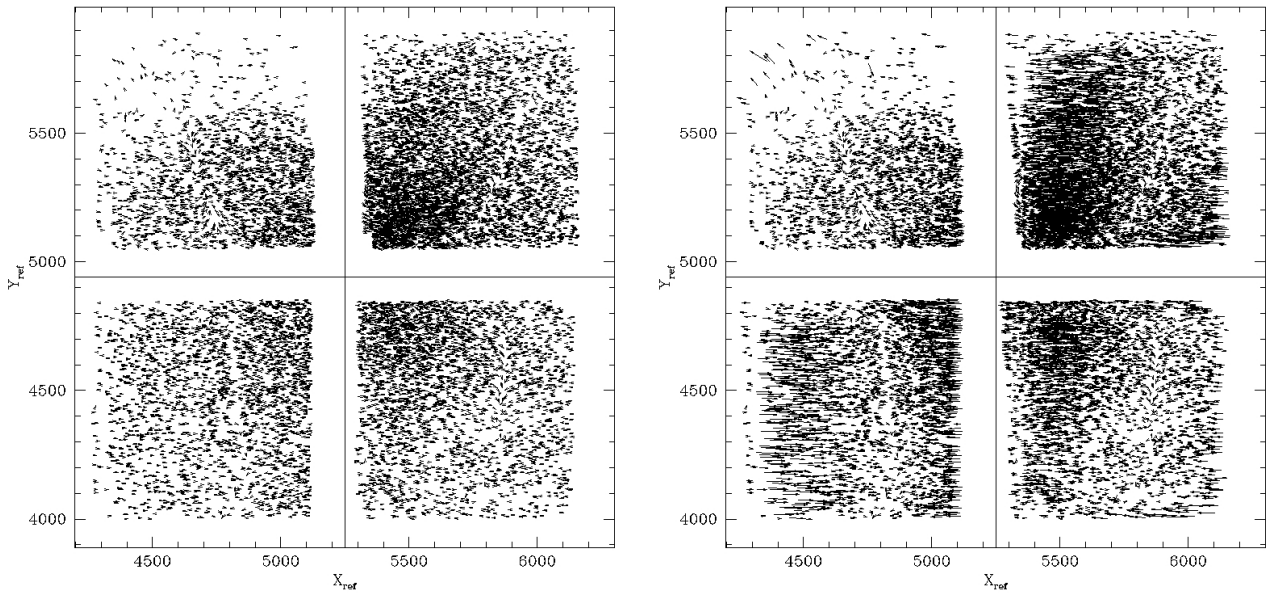

Figure 7. Maps of distortion residuals for one of the K-band exposures. The left panel shows the residuals magnified by the same factor as that used for the distortion maps (20). Instead, the right panel shows them magnified by 80, to enhance the detail.

epoch. Since only stars with an error smaller than 0.03 mas yr^{-1}were used, and the GeMS data were taken 6.9 yr after the first HST epoch, the total contribution due to PM uncertainty is ~ 0.2 mas.

Investigations of the internal dynamics of GCs, which might shed light on fundamental topics such as the presence of intermediate mass black holes or the formation of GC multiple populations (e.g.[26]), require precisions < 0.1 mas/yr. Therefore an accurate modelling of such distortions is fundamental to the success of these studies. The method used throughout this analysis proved efficient in achieving this goal (Massari et al. in prep.) but is limited to cases for which already measured PMs are available at least for the bright stars in the field. Therefore, other solutions still have to be investigated. For example, our group is performing a series of studies aimed at anchoring GeMS astrometry to the distortion free reference frame provided by seeing-limited observations obtained with the FLAMINGOS-2 camera at the Gemini-South telescope. Looking to the future, MICADO astrometry might also require to test the use of calibration masks or methods that do not rely on an absolute distortion correction but on a relative calibration.

ACKNOWLEDGMENTS

We thank Benoit Neichel, Carmelo Arcidiacono, Jessica Lu and Marc Ammons for the useful discussions on the GeMS distortions. Based on observations obtained at the Gemini Observatory and acquired through the Gemini Science Archive. GF and DM has been supported by the FIRB 2013 (MIUR grant RBFR13J716).

REFERENCES

[1] Diolaiti, E., "MAORY: A Multi-conjugate Adaptive Optics RelaY for the E-ELT," *The Messenger* **140**, 28–29 (June 2010).

[2] Massari, D., Bellini, A., Ferraro, F. R., van der Marel, R. P., Anderson, J., Dalessandro, E., and Lanzoni, B., "Hubble Space Telescope Absolute Proper Motions Of NGC 6681 (M70) and the Sagittarius Dwarf Spheroidal Galaxy," *ApJ* **779**, 81 (Dec. 2013).

[3] Neichel, B., Lu, J. R., Rigaut, F., Ammons, S. M., Carrasco, E. R., and Lassalle, E., "Astrometric performance of the Gemini multiconjugate adaptive optics system in crowded fields," *MNRAS* **445**, 500–514 (Nov. 2014).

[4] Ammons, S. M., Neichel, B., Lu, J., Gavel, D. T., Srinath, S., McGurk, R., Rudy, A., Rockosi, C., Marois, C., Macintosh, B., Savransky, D., Galicher, R., Bendek, E., Guyon, O., Marin, E., Garrel, V., and Sivo, G., "A measurement of the systematic astrometric error in GeMS and the short-term astrometric precision in ShaneAO," in [*Adaptive Optics Systems IV*], *Proc. SPIE* **9148**, 91481J (Aug. 2014).

[5] Lu, J. R., Neichel, B., Anderson, J., Sinukoff, E., Hosek, M. W., Ghez, A. M., and Rigaut, F., "Near-infrared astrometry of star clusters with different flavors of adaptive optics and HST," in [*Adaptive Optics Systems IV*], *Proc. SPIE* **9148**, 91480B (July 2014).

[6] Fritz, T. K., Kallivayalil, N., Carrasco, E. R., Neichel, B., Davies, R., Beaton, R., Angell, D., Linden, S., Zivick, P., Majewski, S., Damke, G., Boylan-Kolchin, M., van der Marel, R., and Sohn, T., "Astrometry with MCAO at Gemini and at ELTs," *ArXiv e-prints* (Jan. 2016).

[7] Trippe, S., Davies, R., Eisenhauer, F., Schreiber, N. M. F., Fritz, T. K., and Genzel, R., "High-precision astrometry with MICADO at the European Extremely Large Telescope," *MNRAS* **402**, 1126–1140 (Feb. 2010).

[8] Clenet, Y., Gratadour, D., Gendron, E., Rousset, G., and Sevin, A., "First GPU-based end-to-end AO simulations to dimension the E-ELT MICADO SCAO mode," in [*Proceedings of the Third AO4ELT Conference*], Esposito, S. and Fini, L., eds., 29 (Dec. 2013).

[9] Bellini, A., Anderson, J., van der Marel, R. P., Watkins, L. L., King, I. R., Bianchini, P., Chanamé, J., Chandar, R., Cool, A. M., Ferraro, F. R., Ford, H., and Massari, D., "Hubble Space Telescope Proper Motion (HSTPROMO) Catalogs of Galactic Globular Clusters. I. Sample Selection, Data Reduction, and NGC 7078 Results," *ApJ* **797**, 115 (Dec. 2014).

[10] Watkins, L. L., van der Marel, R. P., Bellini, A., and Anderson, J., "Hubble Space Telescope Proper Motion (HSTPROMO) Catalogs of Galactic Globular Cluster. II. Kinematic Profiles and Maps," *ApJ* **803**, 29 (Apr. 2015).

[11] Fiorentino, G., Ferraro, I., Iannicola, G., Bono, G., Monelli, M., Testa, V., Arcidiacono, C., Faccini, M., Gilmozzi, R., Xompero, M., and Briguglio, R., "On the use of asymmetric PSF on NIR images of crowded stellar fields," in [*Adaptive Optics Systems IV*], *Proc. SPIE* **9148**, 91483U (Aug. 2014).

[12] Saracino, S., Dalessandro, E., Ferraro, F. R., Lanzoni, B., Geisler, D., Mauro, F., Villanova, S., Moni Bidin, C., Miocchi, P., and Massari, D., "GEMINI/GeMS Observations Unveil the Structure of the Heavily Obscured Globular Cluster Liller 1.," *ApJ* **806**, 152 (June 2015).

[13] Turri, P., McConnachie, A. W., Stetson, P. B., Fiorentino, G., Andersen, D. R., Véran, J.-P., and Bono, G., "Toward Precision Photometry for the ELT Era: The Double Subgiant Branch of NGC 1851 Observed with the Gemini/GeMS MCAO System," *ApJL* **811**, L15 (Oct. 2015).

[14] Massari, D., Fiorentino, G., McConnachie, A., Bono, G., Dall'Ora, M., Ferraro, I., Iannicola, G., Stetson, P. B., Turri, P., and Tolstoy, E., "GeMS MCAO observations of the Galactic globular cluster NGC 2808: the absolute age," *A&A* **586**, A51 (Feb. 2016).

[15] Massari, D., Lapenna, E., Bragaglia, A., Dalessandro, E., Contreras Ramos, R., and Amigo, P., "Multiple stellar populations in the globular cluster M3 (NGC 5272): a Strömgren perspective," *MNRAS* **458**, 4162–4171 (June 2016).

[16] Miocchi, P., Lanzoni, B., Ferraro, F. R., Dalessandro, E., Vesperini, E., Pasquato, M., Beccari, G., Pallanca, C., and Sanna, N., "Star Count Density Profiles and Structural Parameters of 26 Galactic Globular Clusters," *ApJ* **774**, 151 (Sept. 2013).

[17] Anderson, J., Sarajedini, A., Bedin, L. R., King, I. R., Piotto, G., Reid, I. N., Siegel, M., Majewski, S. R., Paust, N. E. Q., Aparicio, A., Milone, A. P., Chaboyer, B., and Rosenberg, A., "The Acs Survey of Globular Clusters. V. Generating a Comprehensive Star Catalog for each Cluster," *AJ* **135**, 2055–2073 (June 2008).

[18] Pietrinferni, A., Cassisi, S., Salaris, M., and Castelli, F., "A Large Stellar Evolution Database for Population Synthesis Studies. II. Stellar Models and Isochrones for an α-enhanced Metal Distribution," *ApJ* **642**, 797–812 (May 2006).

[19] Deep, A., Fiorentino, G., Tolstoy, E., Diolaiti, E., Bellazzini, M., Ciliegi, P., Davies, R. I., and Conan, J.-M., "An E-ELT case study: colour-magnitude diagrams of an old galaxy in the Virgo cluster," *A&A* **531**, A151 (July 2011).

[20] Stetson, P. B., "DAOPHOT - A computer program for crowded-field stellar photometry," *PASP* **99**, 191–222 (Mar. 1987).

[21] Greggio, L., Falomo, R., Zaggia, S., Fantinel, D., and Uslenghi, M., "Resolved Stellar Population of Distant Galaxies in the ELT Era," *PASP* **124**, 653–667 (July 2012).

[22] Diolaiti, E., Bendinelli, O., Bonaccini, D., Close, L., Currie, D., and Parmeggiani, G., "Analysis of isoplanatic high resolution stellar fields by the StarFinder code," *A&AS* **147**, 335–346 (Dec. 2000).

[23] Jolissaint, L., Neyman, C., Christou, J., and Wizinowich, P., "Adaptive optics point spread function reconstruction project at W. M. Keck Observatory: first results with faint natural guide stars," in [*Adaptive Optics Systems III*], *Proc. SPIE* **8447**, 844728 (July 2012).

[24] Rigaut, F., Neichel, B., Boccas, M., d'Orgeville, C., Arriagada, G., Fesquet, V., Diggs, S. J., Marchant, C., Gausach, G., Rambold, W. N., Luhrs, J., Walker, S., Carrasco-Damele, E. R., Edwards, M. L., Pessev, P., Galvez, R. L., Vucina, T. B., Araya, C., Gutierrez, A., Ebbers, A. W., Serio, A., Moreno, C., Urrutia, C., Rogers, R., Rojas, R., Trujillo, C., Miller, B., Simons, D. A., Lopez, A., Montes, V., Diaz, H., Daruich, F., Colazo, F., Bec, M., Trancho, G., Sheehan, M., McGregor, P., Young, P. J., Doolan, M. C., van Harmelen, J., Ellerbroek, B. L., Gratadour, D., and Garcia-Rissmann, A., "GeMS: first on-sky results," in [*Adaptive Optics Systems III*], *Proc. SPIE* **8447**, 84470I (July 2012).

[25] Neichel, B., Rigaut, F., Vidal, F., van Dam, M. A., Garrel, V., Carrasco, E. R., Pessev, P., Winge, C., Boccas, M., d'Orgeville, C., Arriagada, G., Serio, A., Fesquet, V., Rambold, W. N., Lührs, J., Moreno, C., Gausachs, G., Galvez, R. L., Montes, V., Vucina, T. B., Marin, E., Urrutia, C., Lopez, A., Diggs, S. J., Marchant, C., Ebbers, A. W., Trujillo, C., Bec, M., Trancho, G., McGregor, P., Young, P. J., Colazo, F., and Edwards, M. L., "Gemini multiconjugate adaptive optics system review - II. Commissioning, operation and overall performance," *MNRAS* **440**, 1002–1019 (May 2014).

[26] Piotto, G., Milone, A. P., Bedin, L. R., Anderson, J., King, I. R., Marino, A. F., Nardiello, D., Aparicio, A., Barbuy, B., Bellini, A., Brown, T. M., Cassisi, S., Cool, A. M., Cunial, A., Dalessandro, E., D'Antona, F., Ferraro, F. R., Hidalgo, S., Lanzoni, B., Monelli, M., Ortolani, S., Renzini, A., Salaris, M., Sarajedini, A., van der Marel, R. P., Vesperini, E., and Zoccali, M., "The Hubble Space Telescope UV Legacy Survey of Galactic Globular Clusters. I. Overview of the Project and Detection of Multiple Stellar Populations," *AJ* **149**, 91 (Mar. 2015).